RSC Advances

ROYAL SOCIETY OF CHEMISTRY

www.rsc.org/advances

Electrodeposition of $ZnCo_2O_4$ nanoparticles for biosensing applications

Kusha Kumar Naik,[a] and Chandra Sekhar Rout,[*a]

[a] School of Basic Sciences, Indian Institute of Technology, Bhubaneswar751013, India

ABSTRACT:

We report the growth of $ZnCo_2O_4$ nanoparticles on indium tin oxide (ITO) coated glass substrates by a simple and highly reproducible electrodeposition method. The as-deposited $ZnCo_2O_4$ nanoparticles are characterized by various structural and microscopical tools for assessing its crystalline and morphological features. Electrochemical sensing properties of the as-prepared $ZnCo_2O_4$ nanoparticles towards glucose and dopamine are studied. $ZnCo_2O_4$ nanoparticles show linear response with respect to change in glucose concentration varying from 10 to 290 μM and possess the LOD value of 36.9 μM and the sensitivity of 0.92 $\mu A \mu M^{-1} cm^{-2}$. In a similar way, $ZnCo_2O_4$ exhibit linear response with respect to change in dopamine concentration varying from 5-100 μM with the LOD value of 15.4 μM and the sensitivity of 0.55 $\mu A \mu M^{-1} cm^{-2}$ respectively.

Keywords: Spinel, Nanoparticles, Electrodeposition, Biosensor

Corresponding author mail: csrout@iitbbs.ac.in (Dr. C.S. Rout)

1. Introduction

$ZnCo_2O_4$ is a regular ternary spinel oxide and is known to exhibit a large degree of cation disorder over the two types of lattice sites, those tetrahedrally or octahedrally by the oxygen.[1,2] It is a promising *p*-type functional material that has been raised considerable interest for potential applications in Li-ion batteries, electrocatalysts and supercapacitors due to their interesting electrochemical and catalytic properties.[2–6] In $ZnCo_2O_4$ crystal, Zn cations occupy the tetrahedral sites while Co cations are evenly distributed to all the octahedral sites, and the anions (O^{-2}) tend to coordinate both the cations Zn^{+2} and Co^{+3}, tetrahedrally and octahedrally respectively to form a close packed FCC structure.[2,7,8]

Fabrication of arrays of nanoparticles have enormous relevance in the fields where important electrochemical processes are involved and the morphology of electrodes strongly affect their performance.[9,10] Assemble nanoarrays possess enhanced reactivity and stability by providing pathways for electrolyte ions and electrons, thereby realizing maximum utilization of electrochemical properties of the material.[11,12] Electrodeposition is the suitable method for nanostructure due to its enhanced driving force. The driving force drives the dissolved ions and atoms towards the substrate and assembles on it creating a suitable morphology and composition of nanostructure which perform novel material properties.[13,14] Electrodeposition takes advantage of charged particles in the solution and is an inexpensive low temperature method to produce uniform films.

Biosensors are becoming essential in the field of health care, chemical and biological analysis ,environmental monitoring, and food processing industries.[15,16]Amongs the biosensors, glucose sensor and dopamine sensors are more important. The amperometric biosensors based on non-enzymatic glucose and dopamine are still challenges to perform better sensitivity, low detection

limit and excellent range of detections. To achieve this goal, one promising way is to employ nanostructure materials, and efforts have been made during the past few decades. [17,18]

In the present study, we prepared thin film of $ZnCo_2O_4$ nanoparticles on ITO coated glass substrates by electrodeposition method. The electrodeposited film exhibited high electrocatalytic activity towards the detection of glucose (GL) and dopamine (DE) molecules.

2. Experimental section

2.1 Synthesis of $ZnCo_2O_4$ nanoparticles

In a typical procedure, the ITO coated glass substrate was thoroughly cleaned with ethanol, acetone and de-ionized water prior to the electrodeposition process. 3 mmol Zn $(NO_3)_2 6H_2O$ and 6 mmol Co $(NO_3)_2 6H_2O$ were dissolved in 10 ml of de-ionized (DI) water and taken in a glass cell. 60 mmol of urea (CH_4N_2O) was slowly added into the solution followed by further addition of 3 mmol potassium chloride (KCl) acting as a supporting electrolyte. The counter electrode (Pt wire), reference electrode (Ag/AgCl) and working electrode (ITO/glass) were dipped into the solution and temperature of the glass cell containing the solution was maintained at 70º C during the electrodeposition process. Electrodeposition was carried out with the help of a Potentiostat/ Galvanostat (Technoscience Ltd., Bangalore, India) by applying a potential of -1.3 V for 180 s with constant stirring of the solution. At high potential and due to the heating of the solution, urea hydrolyzes and helps to nucleate the Zn^{+2} and Co^{+2} ions to form the $ZnCo_2O_4$ nanoparticle. The $ZnCo_2O_4$ nanoparticles uniformly deposited on the surface of conducting substrate and the as-synthesized film was dried naturally then annealed at 500º C for 6 h to achieve better crystallinity.

2.2 Materials characterization

The Crystal structure of the as-synthesized $ZnCo_2O_4$ nanoparticles film was characterized by X-ray diffractometer (Bruker D8 Advanced diffractometer using Cu-Kα radiation (λ = 1.54184 Å)). Morphology and composition of the as-prepared samples were examined by FESEM ((MERLIN Compact with GEMINI I electron column, Zeiss Pvt. Ltd., Germany) equipped with energy dispersive X-ray spectroscopy (EDAX).

2.3 Electrochemical measurement

The electrochemical measurement of the deposited $ZnCo_2O_4$ nanoparticles film was carried out in a same glass cell with three electrodes configuration system. The 0.1 M of NaOH aqueous solution was used as the electrolyte solution to perform the biosensing applications of 0.5 M of glucose and dopamine molecules. The cyclic voltammetric (CV) and chrono-amperometric (CA) experiments were performed in NaOH solution in order to investigate the electrochemical activity of the as-prepared $ZnCo_2O_4$ nanoparticles. For CV experiments, 6 ml of NaOH solution was taken in a same glass cell with three electrodes system and a linear voltage 0 to 0.75 V for glucose study and 0 to 0.7 V for dopamine study were supplied to the electrodes to observe the catalytic behaviour of the $ZnCo_2O_4$ nanoparticles. Then finally, 100 μM of glucose concentrations and dopamine concentrations were added separately to obtain the sensing activities of the $ZnCo_2O_4$ nanoparticles. Similarly, the IT and interference experiment were carried out in a glass cell of three electrodes set up containing 140 ml of NaOH solution. Then the solution was stirred at 1100 rpm and a potential value of 0.4 V was applied to three electrodes .Again for IT measurement, various concentrations (5,10,15,20,30,40,50 μM) of glucose and dopamine molecules were dropped into the solution separately in a interval of 70 s to study the electrochemical response of the synthesized material.

To perform the selectivity of the synthesized material various interfering species like uric acid (UA), lactic acid (LA) and ascorbic acid (AA) were selected then 0.05 M of each interfering species was dissolved in 10 ml of NaOH solution separately in a glass beaker then 10 μM of each species added into the solution periodically in a interval of 70 s.

3. Results and discussion

3.1. Characterization of $ZnCo_2O_4$ nanoparticles

FESEM images of the $ZnCo_2O_4$ nanoparticles are depicted in Fig.1a, and 1b, which show that the as-synthesized thin film consists of spherical structures having 5-10 nm diameters and the nanoparticles are sparsely populated throughout the ITO surface. The nanoparticles are uniformly distributed with precise control over the distribution. The XRD pattern of the $ZnCo_2O_4$ nanoparticles is shown in Fig. 1c and confirms the formation of pure and crystalline phase. The peaks at 2θ = (31.28), (36.85), (44.82), (55.67), (59.37), (65.25) and (68.65) corresponding to the (220), (311), (400), (422), (511), (440) and (531) planes of the standard JCPDS value of spinel $ZnCo_2O_4$ (JCPDS-812295). The peak positioned at 28.70 Å is acquainted to the hydroxide hydrate of Zinc-cobalt oxide (JCPDS-211477). To know the effect of annealing we performed XRD of the as-prepared sample and the data is shown in Fig. S1. No characteristic peak of other compounds was observed indicating that the as-prepared film shows good impurity. EDAX and elemental mapping confirmed the presence of Zn, Co and O confirming the formation of pure $ZnCo_2O_4$ phase, Fig. 1d and Fig. 2. Raman spectra of the $ZnCo_2O_4$ shows characteristic peaks of spinel Zinc cobalt oxide (Fig. S2, Supplementary Information). The peak at 477 and 515 cm^{-1} are assigned to the strong vibrational modes $\boldsymbol{E_g}$ and $\boldsymbol{F_{2g}^{(2)}}$ respectively. The Raman vibrational mode (i.e. $\boldsymbol{A_{1g}}$) results in peak positioned at 686 cm^{-1}.

3.2 Electrochemical sensing towards glucose

3.2.1 Cyclic voltammetric studies

The CVs experiment has been performed in the three electrodes system in a glass cell with the applied potential of 0 to 0.75 V at scan rate 40 mvs^{-1}. During anodic scan, small hump at 0.31 V and broad peak between 0.4 to 0.65 V observed and again peak at 0.45 V and small hump at 0.31 V observed during cathodic scan, Fig. 3a. The redox peak indicated the synthesized material is $ZnCo_2O_4$ nanoparticles.[19–22]

The mechanism and electrochemical catalysis of the $ZnCo_2O_4$ nanoparticles towards glucose molecules can be understood from schematic diagram Fig. 4a and as follows:

During anodic scan: When the voltage applied to the electrodes, the Zn^{+2} and Co^{+2} ion species present on the surface of substrate oxidise to form Zn^{+3} and Co^{+3} ions. Therefore, the oxidation hump at 0.31 V and broad range of oxidation peak 0.4 to 0.65 V observed due to oxidation of Zn^{+2}/Zn^{+3} and Co^{+2}/Co^{3+} cations. [23-25]

$ZnCo_2O_4 + OH^- + H_2O \leftrightarrow Zn(OH)_2 + 2CoOOH + e^-$ ----------(1)

$Zn(II) + Co(II) \leftrightarrow Zn(III) + Co(III) + 2e^-$ ----------(2)

Similarly, when glucose molecules (100 μM) was dropped into the solution, the glucose molecules also oxidised in the applied potential range and transferred to gluconolactone molecules.[22,23]

$Glucose\ (C_6H_{12}O_6) \rightarrow Gluconolactone\ (C_6H_{10}O_6) + 2H^+ + 2e^-$ ----------(3)

The oxidations of metal ions and glucose molecules occur simultaneously at the same applied potential range inside the solution. The electrochemical activity between glucose to

gluconolactone molecule is directly proportional to the oxidation states of Zn and Co species.[24-26] Thus the glucose molecules are responded by the $ZnCo_2O_4$ nanoparticles and the change in oxidation peaks are observed in the same potential range.[19-22] Then 100 µM of glucose concentrations added into the solution respectively. The oxidation peaks and peak currents (I_p) increased successively with the increasing glucose concentration from 100 to 1000 µM in the solution .[24, 26, 29, 30]

During cathodic scan: In the cathodic scan, the applied potential is reversed i.e (0.75 V to 0), therefore, the absorbed electrons are released from $ZnCo_2O_4$ electrode into the solution and reduction peaks are observed.

$Zn\ (III) + Co\ (III) + 2e^{-} \leftrightarrow Zn\ (II\ ) + Co\ (II)$----------(4)

The continuation of the oxidation and reduction of the metal ions present on the $ZnCo_2O_4$ electrode surface determine the sensing of glucose molecules. The sensing of the glucose molecules not only depend on the electrocatalytic behaviour of the metal ions but also the morphology, active edges, crystal structure, dimensions of the nanostructure, composition, pH and chemical environment of the electrolytes.[10,15]

Fig. 3c shows the CVs data of $ZnCo_2O_4$/ITO in 100 µM of glucose concentration at different scan rates. By increasing the scan rate, the amplitude of the redox peak current increases significantly and the oxidation peak position shifted towards positive side and reduction peak position shifted towards negative side. These observations indicate that the oxidation process occurring at the electrode surface is a diffusion controlled process. [23,24]

3.2.2 Chrono-amperometric studies

Chrono-amperometric (IT) response of the $ZnCo_2O_4$ nanoparticles has been carried out in a potential value of 0.4 V under stirring condition at 1100 rpm. When 10 µM of glucose molecules were dropped into the solution, the current rose instantly from the horizontal line and again achieved to horizontal line showing responding time 22 s. Then 10, 20,30,40,50 µM

of glucose molecules were added continuously into the solution at a time interval of 70 s, Fig. 5a. The sensitivity of the $ZnCo_2O_4$/ITO can be calculated by taking into consideration of the calibration graph and it showed linear range of detection 10-290 μM, limit of detection (LOD) 36.9 μM with sensitivity 0.92 μAμMcm^{-2}.

One of the most important analytical factors for an amperometric biosensor is the selectivity of the sensor towards target analytes. The interference study has been carried out at 0.4 V potential under the same experimental condition in the glass cell by adding the 10 μM of UA, DA, LA and AA continuously into the solution in the 70 s time interval which is shown in Fig. 5c. It is observed that the selectivity of the sensor is good even in the presence of interfering species. To investigate the reproducibility of the $ZnCo_2O_4$ electrode, five independently fabricated electrodes were tested for glucose sensing and it showed an acceptable reproducibility with a relative standard deviation of 3.1% for the current determined at a glucose concentration of 10 μM. The stability of the sensor performance was tested by monitoring the remaining amount of current response after successive cycling of the electrode for 5000 circles in the same applied potential at 100 mV/s scan rate. The material exhibited about 80% stability (Fig. S5)

3.3 Electrochemical dopamine sensing

3.3.1 Cyclic voltammetric studies

The CVs experiment for dopamine study has been performed at 0 to 0.7 V at 40 mV/s scan rate and it is observed that when 100 μM dopamine molecules was added into the solution, two distinct peaks at 0.31 V and broad peak 0.4 to 0.65 V appeared. The peak at 0.31 V and broad peak from 0.4 to 0.65 V range corresponds to the redox reaction of $ZnCo_2O_4$ nanoparticle.[25–29]

The electrochemical reaction and the mechanism behind dopamine sensing can be explained using eq^{n} (1), (2) and (4) and its schematic diagram, Fig. 4a.

Dopamine ($C_8H_{11}NO_2$) $\rightarrow C_8H_9NO_2 + 2H^+ + 2e^-$----------(5)

The hydrogen atoms attach with the dopamine molecule partially breaks down in the applied potential range and release two electrons into the solution (eqn-5 and Fig. 4c). These two electrons released from each dopamine molecules lead towards increasing of oxidation peak current (I_p). The peak current increased successively with addition of dopamine concentrations from 100 µM to 1000 µM which demonstrate the linear response of $ZnCo_2O_4$ nanoparticles.[21,22,30,31, 40]

The CVs of the $ZnCo_2O_4$/ITO at different scan rates in the presence of 100 µM dopamine molecules has been performed and shown in Fig. 6c. Both the oxidation and reduction peak currents increased linearly with the increase in scan rates which clearly indicated that the oxidation reaction occurred on the electrode surface is diffusion controlled process.[19,20,32,33]

3.3.2 Chrono-amperometric studies

The CA studies of dopamine molecules have been executed in the same parameters When 5 µM of dopamine molecule was added into the solution the current value increased instantly from horizontal line showing its response time 20 s, Fig. 7d.Then the various concentrations of dopamine molecules added in to the solutions in the interval of 70 s. The calibration graph is shown in Fig. 7b which indicates that the sensor possesses a linear range of detection from 5 -100 µM with the sensitivity value of 0.55 $\mu A \mu M^{-1} Cm^{-2}$ and the LOD value of 15.4 µM.

The interference effect of the $ZnCo_2O_4$/ITO towards dopamine sensing in the presence of interference species has been carried out and is shown in Fig. 7c. The stability of the $ZnCo_2O_4$/ITO towards dopamine sensing has been ascertained by performing CV of 500 cycles

in the presence of 100 μM dopamine molecules (Fig. S5). It is observed that $ZnCo_2O_4$/ITO exhibited good stability by achieving ~82 % of the initial current after 5000 cycles. For real sample application of the $ZnCo_2O_4$/ITO, the CVs and CAs experiment have been carried out in sodium phosphate buffer solution (PBS) with pH which is shown in Fig. S3.

4. Conclusions

Thin films of $ZnCo_2O_4$ nanostructure have been deposited onto an ITO substrate by a facile low-temperature and cost effective electrodeposition method. The nanoparticles are pure in form, uniform and sparsely populated over ITO surface having nanoparticle size 5-10 nm. The electrochemical sensing properties of $ZnCo_2O_4$ nanoparticle towards glucose and dopamine were investigated. Large surface area of the deposited nanoparticles and enhanced electrochemical properties due to the large number of active sites played vital role for the detection of low concentration of glucose and dopamine molecules. The $ZnCo_2O_4$ nanoparticle electrode based sensor exhibited high sensitivity of 0.92 $\mu A \mu M cm^{-2}$ with a LOD 36.9 μM for glucose and sensitivity of 0.55 $\mu A \mu M^{-1} cm^{-2}$ and the LOD 15.4 μM for dopamine molecules. Hence, $ZnCo_2O_4$ nanoparticle prepared by cost effective electrodeposition method paves the way for the development of glucose and dopamine sensors.

References

1 P. F. Ndione, Y. Shi, V. Stevanovic, S. Lany, A. Zakutayev, P. A. Parilla, J. D. Perkins, J. J. Berry, D. S. Ginley and M. F. Toney, *Adv. Funct. Mater.*, 2014, **24**, 610–618.

2 T. W. Kim, M. A. Woo, M. Regis and K.-S. Choi, *J. Phys. Chem. Lett.*, 2014, **5**, 2370–2374.

3 M. A. Woo, M.-S. Song, T. W. Kim, I. Y. Kim, J.-Y. Ju, Y. S. Lee, S. J. Kim, J.-H. Choy and S.-J. Hwang, *J. Mater. Chem.*, 2011, **21**, 4286–4292.

4 D. Cai, H. Huang, D. Wang, B. Liu, L. Wang, Y. Liu, Q. Li and T. Wang, *ACS Appl. Mater. Interfaces*, 2014, **6**, 15905–15912.

5 Y. Qiu, S. Yang, H. Deng, L. Jin and W. Li, *J. Mater. Chem.*, 2010, **20**, 4439–4444.

6 F. M. Courtel, H. Duncan, Y. Abu-Lebdeh and I. J. Davidson, *J. Mater. Chem.*, 2011, **21**, 10206–10218.

7 K. K. and P. Konstantinov, *J. Phys. Condens. Matter*, 1993, **5**, 9287.

8 S. Ratha, R. T. Khare, M. A. More, R. Thapa, D. J. Late and C. S. Rout, *RSC Adv.*, 2015, **5**, 5372–5378.

9 K. Tian, M. Prestgard and A. Tiwari, *Mater. Sci. Eng. C*, 2014, **41**, 100–118.

10 S. K. Arya, S. Saha, J. E. Ramirez-Vick, V. Gupta, S. Bhansali and S. P. Singh, *Anal. Chim. Acta*, 2012, **737**, 1–21.

11 C. J. Murphy, T. K. Sau, A. M. Gole, C. J. Orendorff, J. Gao, L. Gou, S. E. Hunyadi and T. Li, *J. Phys. Chem. B*, 2005, **109**, 13857–13870.

12 M. Zhang, G. Zuo, Z. Zong, H. Cheng, Z. He, C. Yang and G. Zou, *Small*, 2006, **2**, 727–731.

13 V. Armel, O. Winther-Jensen, R. Kerr, D. R. MacFarlane and B. Winther-Jensen, *J. Mater. Chem.*, 2012, **22**, 19767–19773.

14 J. Sun, X. Liu, L. Meng, W. Wei and Y. Zheng, *Langmuir*, 2014, **30**, 11002–11010.

15 M. Ahmad, C. Pan, Z. Luo and J. Zhu, *J. Phys. Chem. C*, 2010, **114**, 9308–9313.

16 N. A. Rakow and K. S. Suslick, *Nature*, 2000, **406**, 710–713.

17 J. Zhao, F. Wang, J. Yu and S. Hu, *Talanta*, 2006, **70**, 449–454.

18 H. Zhou, H. Chen, S. Luo, J. Chen, W. Wei and Y. Kuang, *Biosens. Bioelectron.*, 2005, **20**, 1305–1311.

19 X.-C. Dong, H. Xu, X.-W. Wang, Y.-X. Huang, M. B. Chan-Park, H. Zhang, L.-H. Wang, W. Huang and P. Chen, *ACS Nano*, 2012, **6**, 3206–3213.

20 C.-W. Kung, C.-Y. Lin, Y.-H. Lai, R. Vittal and K.-C. Ho, *Biosens. Bioelectron.*, 2011, **27**, 125–131.

21 I. G. Casella and M. Gatta, *J. Electroanal. Chem.*, 2002, **534**, 31–38.

22 Y. Ding, Y. Wang, L. Su, M. Bellagamba, H. Zhang and Y. Lei, *Biosens. Bioelectron.*, 2010, **26**, 542–548.

23 Y. Zou, L. He, K. Dou, S. Wang, P. Ke and A. Wang, *RSC Adv.*, 2014, **4**, 58349–58356.

24 R. K. Srivastava, S. Srivastava, T. N. Narayanan, B. D. Mahlotra, R. Vajtai, P. M. Ajayan and A. Srivastava, *ACS Nano*, 2012, **6**, 168–175.

25 T. Kong, Y. Chen, Y. Ye, K. Zhang, Z. Wang and X. Wang, *Sensors Actuators B Chem.*, 2009, **138**, 344–350.

26 Y.-T. Wang, L. Yu, Z.-Q. Zhu, J. Zhang, J.-Z. Zhu and C. Fan, *Sensors Actuators B Chem.*, 2009, **136**, 332–337.

27 J. X. Wang, X. W. Sun, A. Wei, Y. Lei, X. P. Cai, C. M. Li and Z. L. Dong, *Appl. Phys. Lett.*, 2006, **88**, -.

28 X. Liu, Z. Chang, L. Luo, T. Xu, X. Lei, J. Liu and X. Sun, *Chem. Mater.*, 2014, **26**, 1889–1895.

29 S. Palmas, F. Ferrara, A. Vacca, M. Mascia and A. M. Polcaro, *Electrochim. Acta*, 2007, **53**, 400–406.

30 C. Xia, N. Wang, L. Wang and L. Guo, *Sensors Actuators B Chem.*, 2010, **147**, 629–634.

31 L. Fang, K. Huang, B. Zhang, B. Liu, Y. Liu and Q. Zhang, *RSC Adv.*, 2014, **4**, 48986–48993.

32 C. L. Weaver, H. Li, X. Luo and X. T. Cui, *J. Mater. Chem. B*, 2014, **2**, 5209–5219.

33 I. de O. Matos and W. A. Alves, *ACS Appl. Mater. Interfaces*, 2011, **3**, 4437–4443.

34 G. Vijayaprasath, R. Murugan, J. Shankara Narayanan, V. Dharuman, G. Ravi and Y. Hayakawa, *J. Mater. Sci. Mater. Electron.*, 2015, **26**, 4988–4996.

35 Z. W. Zhao, X. J. Chen, B. K. Tay, J. S. Chen, Z. J. Han and K. A. Khor, *Biosens. Bioelectron.*, 2007, **23**, 135–139.

Table-1: Comparison of glucose sensor performance of zinc oxide based material with the present work

Electrodes	Sensitivity	Linear range	Limit of detection (LOD)	Response time	References
Co doped ZnO nanoparticle	-	32 mM	5 µM	4s	[34]
ZnO: Co	13.3 µA/mAcm^2	0-4 mM	20 µM	8 s	[35]
$ZnCo_2O_4$	0.92 µAµM^{-1}cm^{-2}	10-290 µM	36.9 µM	22 s	Present work

Table -2: Dopamine sensor performance of $ZnCo_2O_4$ nanoparticles.

Electrodes	Sensitivity	Linear range	Limit of detection (LOD)	Response time	References
$ZnCo_2O_4$	0.51 µAµM^{-1}cm^{-2}	10-100 µM	15.4 µM	20 s	Present work

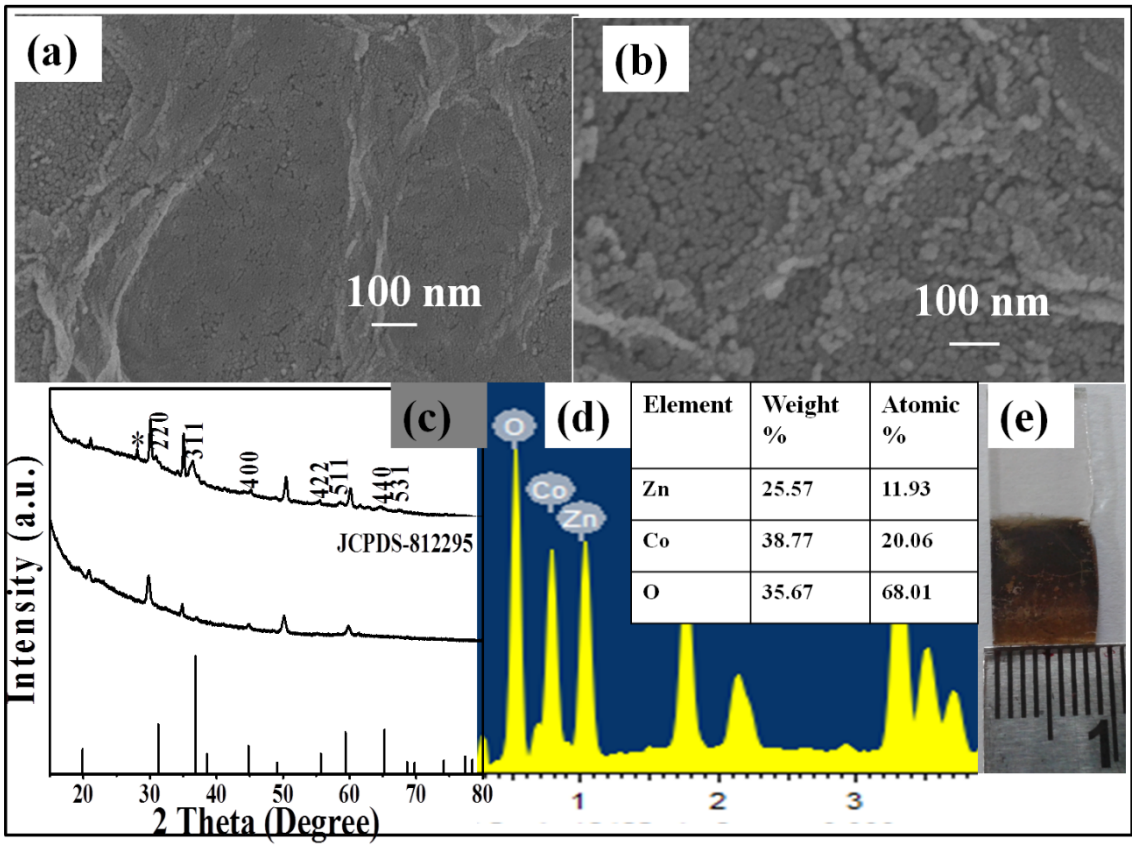

Fig. 1 (a) Low and (b) high magnification SEM images of $ZnCo_2O_4$ thin film nanoparticles on ITO coated glass substrate with the inset in (a) showing optical image of an as-prepared thin film sample. (c) XRD pattern and (d) EDAX pattern with percentage of the elements of the $ZnCo_2O_4$ nanoparticles.

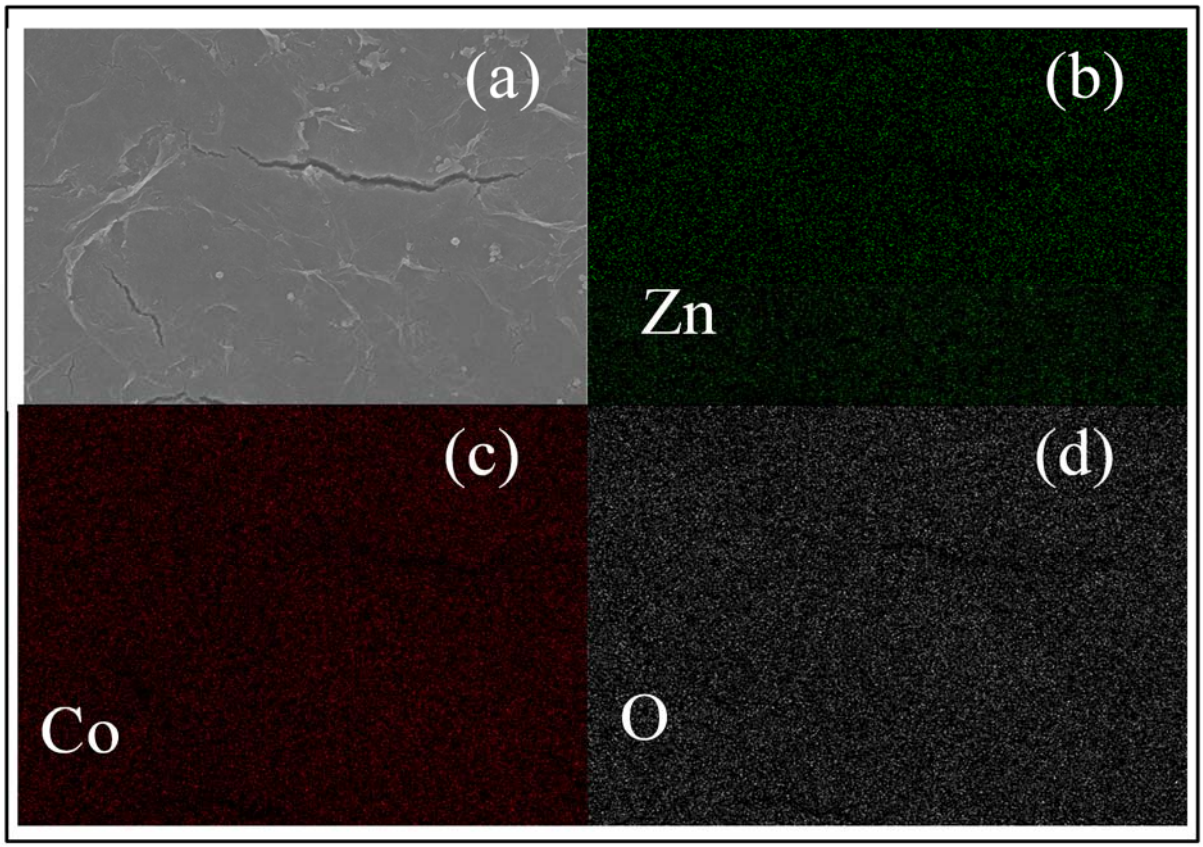

Fig. 2 (a) SEM images of the large area thin film of $ZnCo_2O_4$ nanoparticles, corresponding elemental mapping of the elements; (b) Zn, (c) Co, and (d) O respectively.

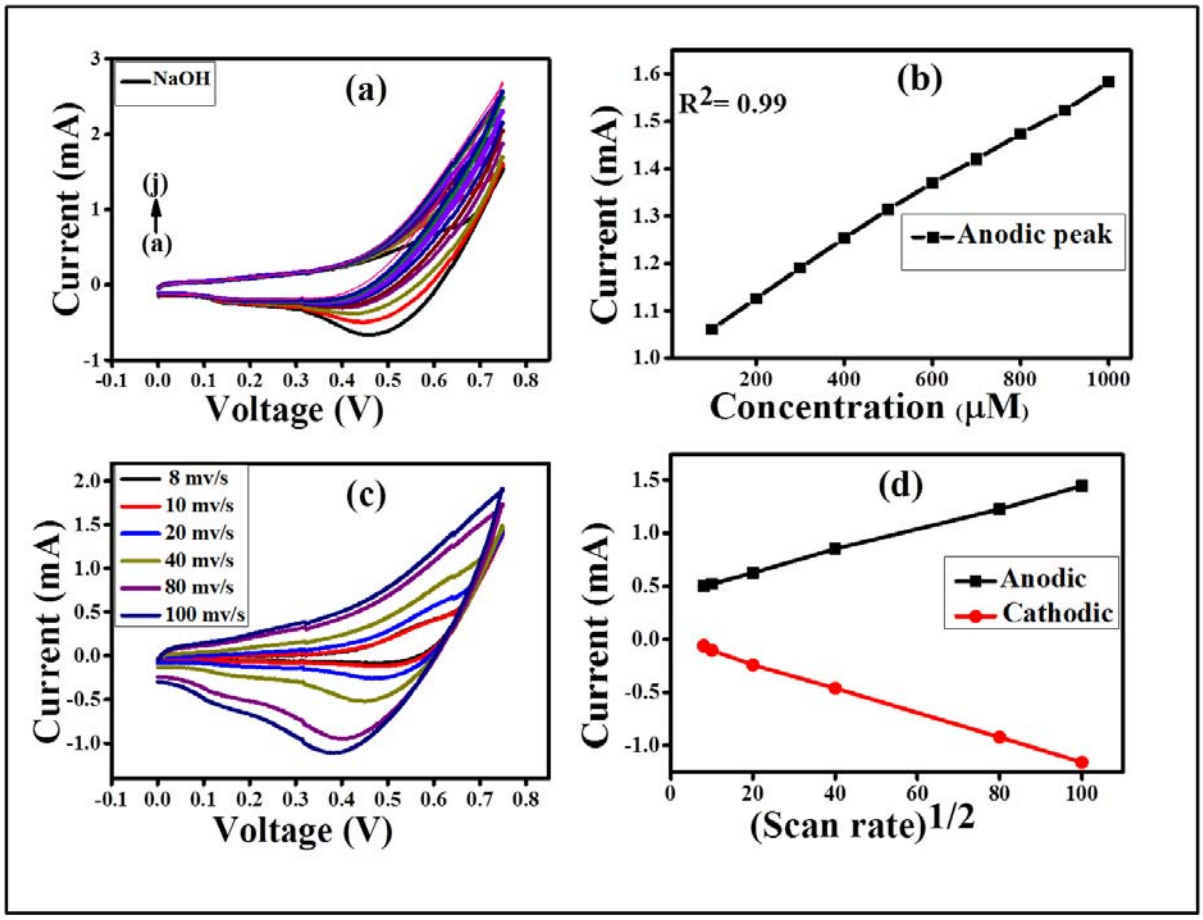

Fig. 3 (a) CVs of $ZnCo_2O_4$ nanoparticles in 0.1 M NaOH with different concentration of glucose (concentration of glucose varies from 100 μM to 1000 μM). (b) Obtained anodic peak current against different concentration of glucose molecules. (c) CVs at different scan rates in the presence of 100 μM glucose, (d) change in glucose oxidation and reduction peak current against square root of scan rate.

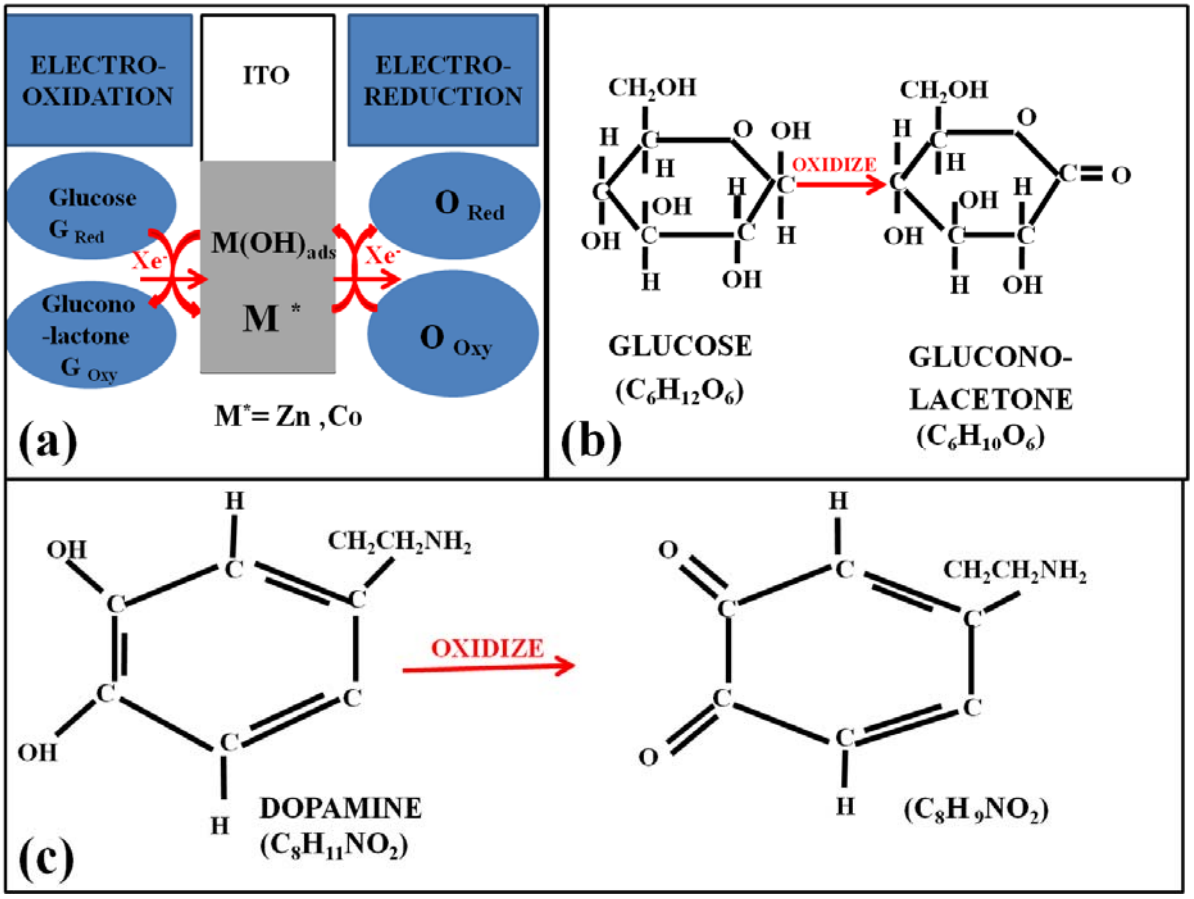

Fig. 4 (a) Schematic representation of the glucose and dopamine sensing mechanism, (b) structural representation of the glucose and gluconolactone molecule, (c) structural representation of dopamine and its oxidation state of dopamine molecules.

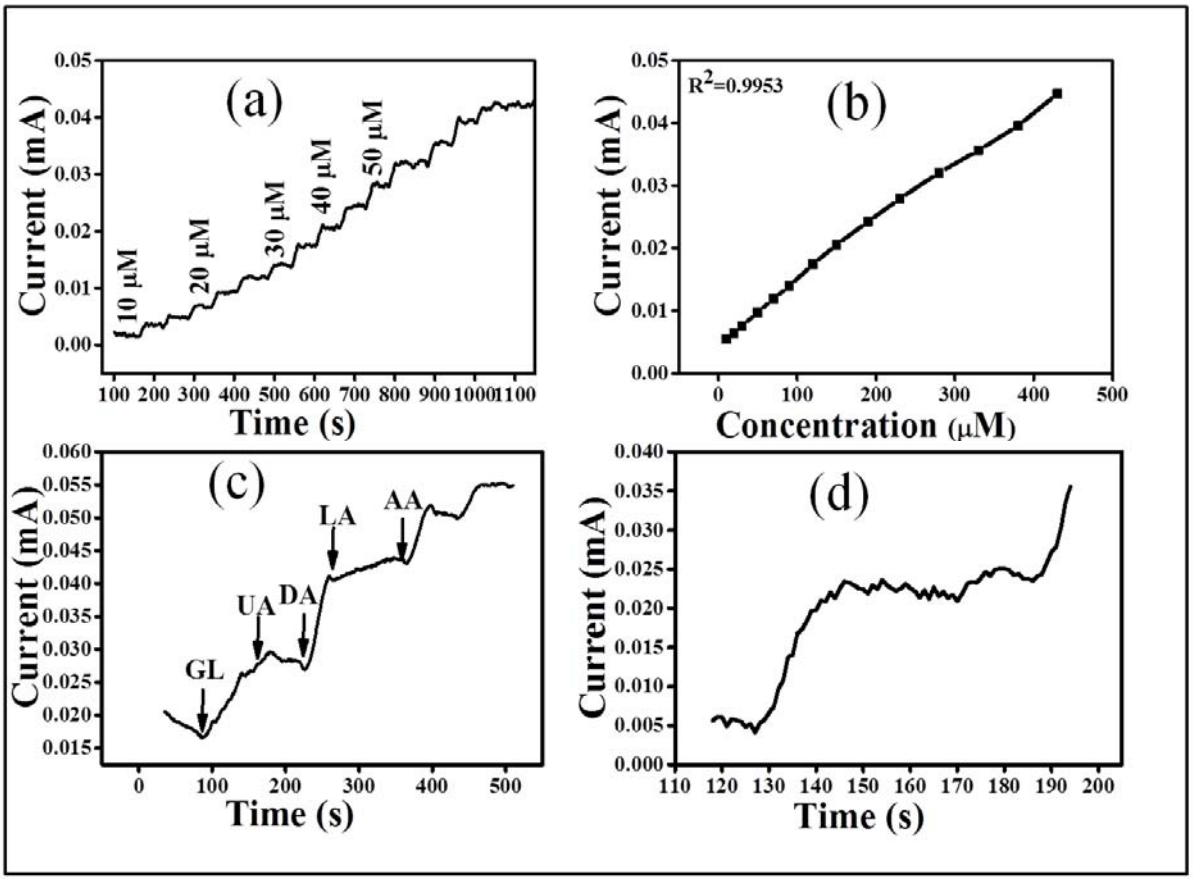

Fig. 5 (a) CA response of $ZnCo_2O_4$ nanoparticles with successive addition of glucose molecules in 0.1 M NaOH solution at 0.4 V, (b) calibration plot for glucose sensor, (c) interference study of $ZnCo_2O_4$ nanoparticles and (d) response curve.

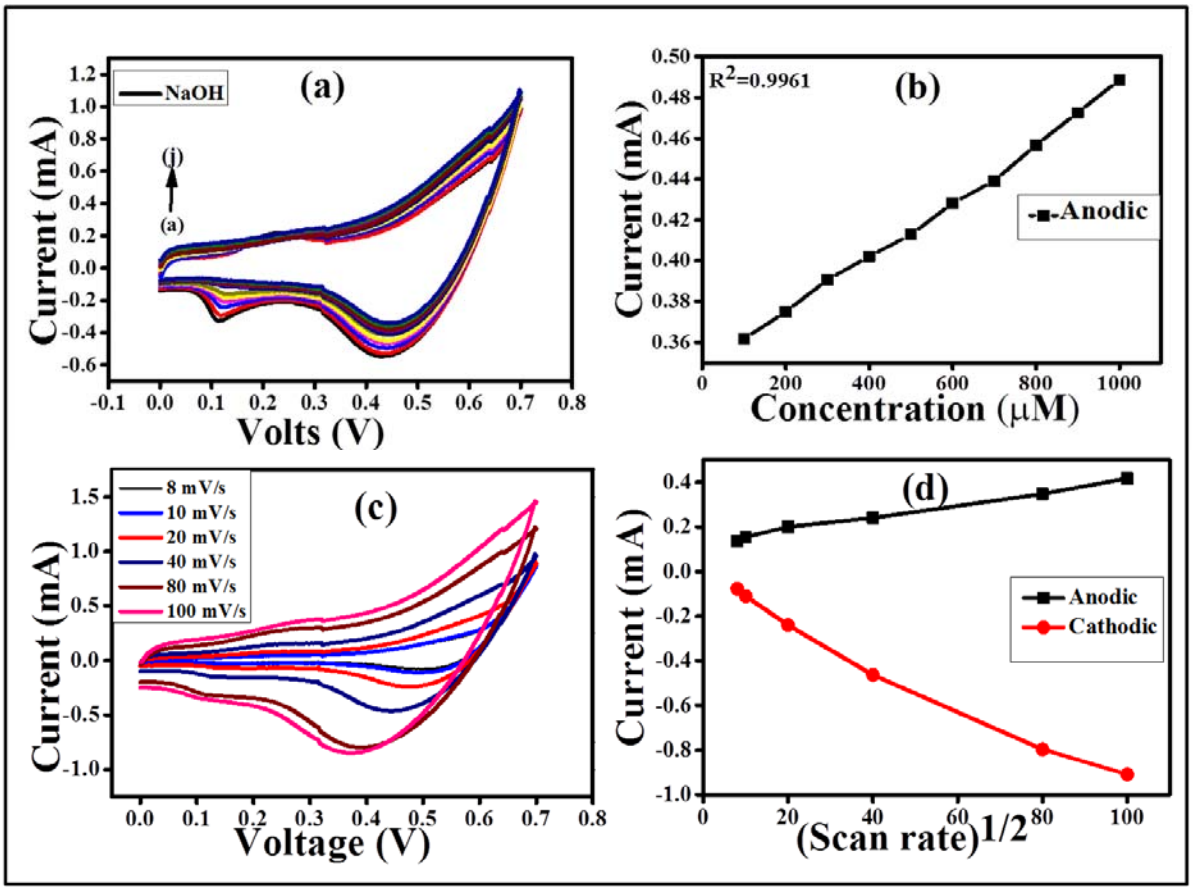

Fig. 6 (a) CVs of $ZnCo_2O_4$ nanoparticles in 0.1 M NaOH solution with different concentration of dopamine (concentration of glucose varies from 100 μM to 1000 μM). (b) Obtained anodic peak current against different concentration of dopamine. (c) CVs at different scan rates in the presence of 100 μM dopamine, (d) change in oxidation and reduction peak current against square root of scan rate.

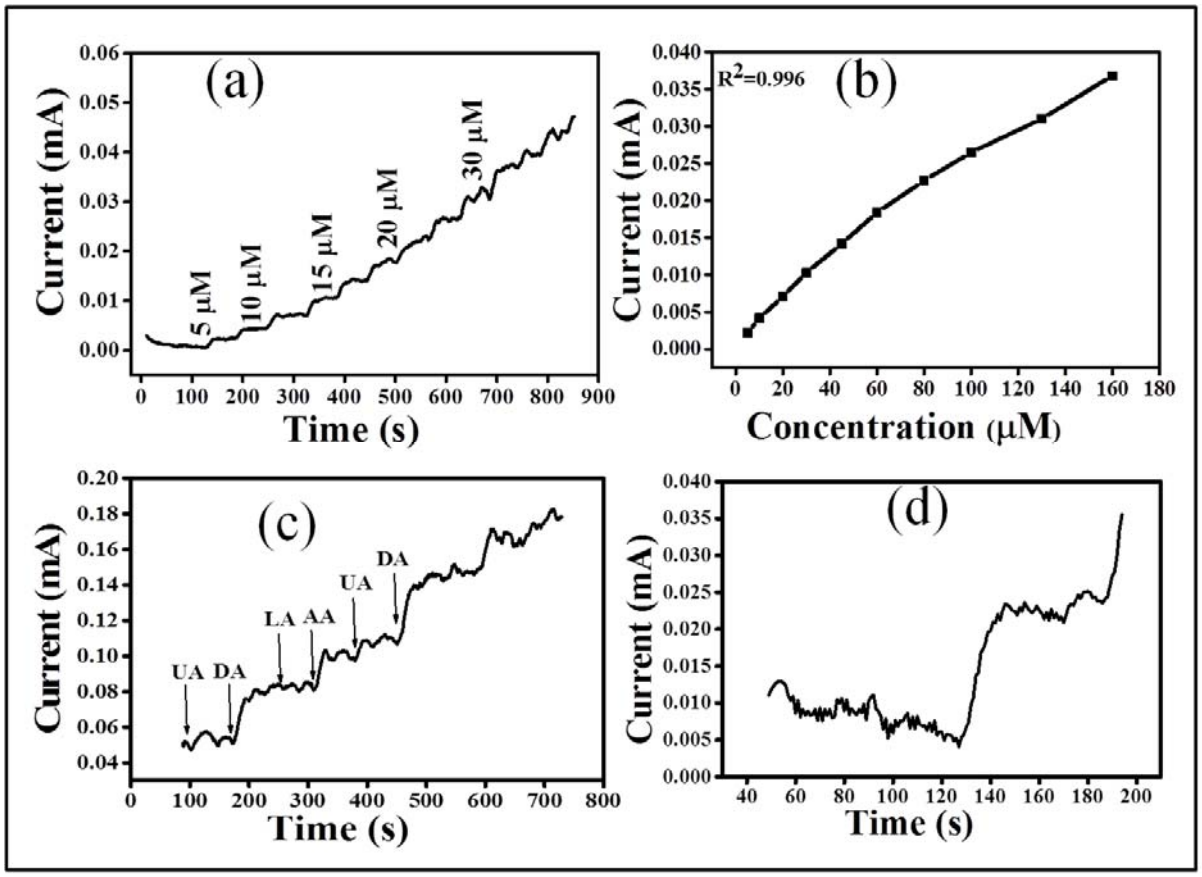

Fig. 7 (a) Chrono-amperometric response of $ZnCo_2O_4$ nanoparticle with successive addition of dopamine molecule in the presence of 0.1 M NaOH solution at 0.4 V, (b) calibration plot for dopamine, (c) interference study (d) response curve.